BioCore Exploring Scientific Community

International Journal of Biotechnology and Bioengineering

Research Article ISSN 2475-3432

Seismo Magnetic Field Fractal Dimension for Characterizing Shajara Reservoirs of the Permo-Carboniferous Shajara Formation, Saudi Arabia

Prof. Khalid Elyas Mohamed Elameen Alkhidir, ph.D.

Department of Petroleum and Natural Gas Engineering, College of Engineering, King Saud University, Saudi Arabia

Abstract

The quality and assessment of a reservoir can be documented in details by the application of Seismo magnetic field. This research aims to calculate fractal dimension from the relationship among Seismo magnetic field, maximum Seismo magnetic field and wetting phase saturation and to approve it by the fractal dimension derived from the relationship among capillary pressure and wetting phase saturation. In this research, porosity was measured on real collected sandstone samples and permeability was calculated theoretically from capillary pressure profile measured by mercury intrusion contaminating the pores of sandstone samples in consideration. Two equations for calculating the fractal dimensions have been employed. The first one describes the functional relationship between wetting phase saturation, Seismo magnetic field, maximum Seismo magnetic field and fractal dimension. The second equation implies to the wetting phase saturation as a function of capillary pressure and the fractal dimension. Two procedures for obtaining the fractal dimension have been utilized. The first procedure was done by plotting the logarithm of the ratio between Seismo magnetic field and maximum Seismo magnetic field versus logarithm wetting phase saturation. The slope of the first procedure = 3- Df (fractal dimension). The second procedure for obtaining the fractal dimension was determined by plotting the logarithm of capillary pressure versus the logarithm of wetting phase saturation. The slope of the second procedure = Df -3. On the basis of the obtained results of the fabricated stratigraphic column and the attained values of the fractal dimension, the sandstones of the Shajara reservoirs of the Shajara Formation were divided here into three units. The obtained units from bottom to top are: Lower, Middle and Upper Shajara Seismo magnetic field Fractal Dimension Units. It was found that fractal dimension increases with increasing grain size and permeability.

Keywords: Shajara Reservoirs, Shajara Formation, Seismo magnetic field fractal dimension, Capillary pressure fractal dimension

Corresponding author: **Khalid Elyas Mohamed Elameen Alkhidir**

Department of Petroleum and Natural Gas Engineering, College of Engineering, King Saud University, Saudi Arabia

Email: kalkhidir@ksu.edu.sa

Citation: Khalid Elyas Mohamed Elameen Alkhidir (2019), Seismo Magnetic Field Fractal Dimension for Characterizing Shajara Reservoirs of the Permo-Carboniferous Shajara Formation, Saudi Arabia. Int J Biotech & Bioeng. 5:1, 01-08

Received: February 12 2019

Accepted: February 21, 2019

Published: March 28 , 2019

Introduction

Seismo electric effects related to electro kinetic potential, dielectric permitivity, pressure gradient, fluid viscosity, and electric conductivty was first reported by [1]. Capillary pressure follows the scaling law at low wetting phase saturation was reported by [2]. Seismo electric phenomenon by considering electro kinetic coupling coefficient as a function of effective charge density, permeability, fluid viscosity and electric conductivity was reported by [3]. The magnitude of seismo electric current depends porosity, pore size, zeta potential of the pore surfaces, and elastic properties of the matrix was investigated by [4]. The tangent of the ratio of converted electic field to pressure is approximately in inverse proportion to permeability was studied by [5]. Permeability inversion from seismoelectric log at low frequency was studied by [6]. They reported that, the tangent of the ratio among electric excitation intensity and pressure field is a function of porosity, fluid viscosity, frequency, tortuosity, fluid density and Dracy permeability. A decrease of seismo electric frequencies with increasing water content was reported by [7]. An increase of seismo electric transfer function with increasing water saturation was studied by [8]. An increase of dynamic seismo electric transfer function with decreasing fluid conductivity was described by [9]. The amplitude of seismo electric signal increases with increasing permeability which means that the seismo electric effects are directly related to the permeability and can be used to study the permeability of the

reservoir was illustrated by [10]. Seismo electric coupling is frequency dependent and decreases expontialy when frequency increases was demonstrated by [11]. An increase of permeability with increasing pressure head and bubble pressure fractal dimension was reported by [12,13]. An increase of geometric and arithmetic relaxtion time of induced polarization fractal dimension with permeability increasing and grain size was described by [14,15,16]. An increase of seismo electric field fractal dimension with increasing permeability and grain size was described by [17]. An increase of resistivity fractal dimension with increasing permeability and grain size was illustrated by [18]. An increase of electro kinetic fractal dimension with increasing permeability and grain size was demonstrated by[19]. An increase of electric potential energy with increasing permeability and grain size was defined by [20] . An increase of electric potential gradient fractal dimension with increasing permeability and grain size was defined by [21]. An increase of differential capacity fractal dimension with increasing permeability and grain size was described by [22].

Material and Method

Sandstone samples were collected from the surface type section of the Permo-Carboniferous Shajara Formation, latitude 26° 52' 17.4", longitude 43° 36' 18. " (Figure1). Porosity was measured on collected samples using mercury intrusion Porosimetry and permeability was derived from capillary pressure data. The purpose of this paper is to obtain seismo magnetic field fractal dimension and to confirm it by capillary pressure fractal dimension. The fractal dimension of the first procedure is determined from the positive slope of the plot of logarithm of the ratio of seismo magnetic field to maximum seismo magnetic field log (H1/2/H1/2max) versus log wetting phase saturation (logSw). Whereas the fractal dimension of the second procedure is determined from the negative slope of the plot of logarithm of log capillary pressure (log Pc) versus logarithm of wetting phase saturation (log Sw).

The seismo magnetic field can be scaled as

$$Sw = \left[\frac{H_{s,r}^{\frac{1}{2}}}{H_{S,r,max}^{\frac{1}{2}}}\right]^{[3-Df]} \quad (1)$$

Where Sw the water saturation, H the seismo magnetic field in ampere / meter generated from the shear wave velocity, Hmax the maximum seismo magnetic field in ampere / meter generated from the shear wave velocity, and Df the fractal dimension.

"Eq. (1)" can be proofed from

$$H_{S,\theta} = \left[\frac{\Phi * \varepsilon 0 * kf * \zeta * \rho f \sqrt{\frac{G}{\rho}} * \frac{dU_{S,r}}{dt}}{\alpha_{\infty} * \eta}\right] \quad (2)$$

Where HS,ɵ the seismo magnetic field generated from shear wave velocity in ampere / meter, Φ the porosity, ε0 permittivity of free scape in Faraday / meter, kf dielectric constant of the fluid, ζ the zeta potential in volt, ρf the fluid density in kilo gram /meter, G the shear modulus in pascal, ρ bulk density in kilo gram /m3, dUS,r /dt the radial grain velocity in meter / second, α∞ the tortuosity, and η the fluid viscosity in pascal * second. The zeta potential can be scaled as

$$\zeta = \left[\frac{C_S * \sigma f * \eta}{\varepsilon f}\right] \quad (3)$$

Where ζ the zeta potential in volt, CS streaming potential coefficient in volt /pascal, σf the fluid electric conductivity in Siemens /meter, η the fluid viscosity in pascal * second, εf the fluid permittivity in Faraday / meter.

Insert "Eq. (3)" "Eq. (2)"

$$H_{S,\theta} = \left[\frac{\Phi * \varepsilon 0 * kf * C_S * \sigma f * \eta * \rho f \sqrt{\frac{G}{\rho}} * \frac{dU_{S,r}}{dt}}{\alpha_{\infty} \varepsilon f * \eta}\right] \quad (4)$$

The streaming potential coefficient can be scaled as

$$C_S = \left[\frac{reff^2 * C_E}{8 * \sigma f * \eta}\right] \quad (5)$$

Where CS the streaming potential coefficient in volt /pascal, reff the effective pore radius in meter, CE the electro osmosis coefficient in pascal / volt, σf the fluid conductivity in Siemens /meter, and η the fluid viscosity in pascal *second.

Insert "Eq. (5)" into "Eq. (4)"

$$H_{S,\theta} = \left[\frac{\Phi * \varepsilon 0 * kf * reff^2 * C_E \sigma f * \eta * \rho f \sqrt{\frac{G}{\rho}} * \frac{dU_{S,r}}{dt}}{\alpha_{\infty} \varepsilon f * \eta * 8 * \sigma f * \eta}\right] \quad (6)$$

If the pore radius is introduced equation 6 will become

$$H_{S,\theta} = \left[\frac{\Phi * \varepsilon 0 * kf * r^2 * C_E * \sigma f * \eta * \rho f \sqrt{\frac{G}{\rho}} * \frac{dU_{S,r}}{dt}}{\alpha_{\infty} \varepsilon f * \eta * 8 * \sigma f * \eta}\right] \quad (7)$$

The maximum pore radius can be scaled as

$$H_{S,r,max} = \left[\frac{\Phi * \varepsilon 0 * kf * r_{max}^2 * C_E * \sigma f * \eta * \rho f \sqrt{\frac{G}{\rho}} * \frac{dU_{S,r}}{dt}}{\alpha_{\infty} \varepsilon f * \eta * 8 * \sigma f * \eta}\right] \quad (8)$$

Divide "Eq. (7)" by "Eq. (8)"

$$\left[\frac{H_{S,\theta}}{H_{S,r,max}}\right] = \left[\frac{\left[\frac{\Phi * \varepsilon 0 * kf * r^2 * C_E * \sigma f * \eta * \rho f \sqrt{\frac{G}{\rho}} * \frac{dU_{S,r}}{dt}}{\alpha_{\infty} \varepsilon f * \eta * 8 * \sigma f * \eta}\right]}{\left[\frac{\Phi * \varepsilon 0 * kf * r_{max}^2 * C_E * \sigma f * \eta * \rho f \sqrt{\frac{G}{\rho}} * \frac{dU_{S,r}}{dt}}{\alpha_{\infty} \varepsilon f * \eta * 8 * \sigma f * \eta}\right]}\right] \quad (9)$$

"Eq. (9)" after simplification will become

$$\left[\frac{H_{S,\theta}}{H_{S,r,max}}\right] = \left[\frac{r^2}{r_{max}^2}\right] \quad (10)$$

Take the square root of "Eq. (10)"

$$\sqrt{\left[\frac{H_{S,\theta}}{H_{S,r,max}}\right]} = \sqrt{\left[\frac{r^2}{r_{max}^2}\right]} \quad (11)$$

"Eq. (11)" after simplification will become

$$\left[\frac{H_{S,\theta}{}^{\frac{1}{2}}}{H_{S,r,max}{}^{\frac{1}{2}}}\right] = \left[\frac{r}{r_{max}}\right] \quad (12)$$

Take the logarithm of "Eq. (12)"

$$\log\left[\frac{H_{S,\theta}{}^{\frac{1}{2}}}{H_{S,r,max}{}^{\frac{1}{2}}}\right] = \log\left[\frac{r}{r_{max}}\right] \quad (13)$$

$$\text{But; } \log\left[\frac{r}{r_{max}}\right] = \frac{\log Sw}{[3-Df]} \quad (14)$$

Insert "Eq. (14)" into "Eq. (13)"

$$\frac{\log Sw}{[3-Df]} = \log\left[\frac{H_{S,\theta}{}^{\frac{1}{2}}}{H_{S,r,max}{}^{\frac{1}{2}}}\right] \quad (15)$$

After log removal "Eq. (15)" will become

$$Sw = \left[\frac{H_{S,\theta}{}^{\frac{1}{2}}}{H_{S,r,max}{}^{\frac{1}{2}}}\right]^{[3-Df]} \quad (16)$$

"Eq. (16)" the proof of equation 1 which relates the water saturation, seismo magnetic field, maximum seismo magnetic field generated from the shaer wave and the fractal dimension.

The capillary pressure can be scaled as

$$Sw = [Df - 3] * Pc * constant \quad (17)$$

Where Sw the water saturation, Pc the capillary pressure and Df the fractal dimension.

Results and Discussion

Based on field observation the Shajara Reservoirs of the Permo-Carboniferous Shajara Formation were divided here into three units as described in Figure1.These units from bottom to top are: Lower Shajara Reservoir, Middle Shajara reservoir, and Upper Shajara Reservoir. Their acquired results of the seismo magnetic field fractal dimension and capillary pressure fractal dimension are displayed in Table 1. Based on the attained results it was found that the seismo magnetic field fractal dimension is equal to the capillary pressure fractal dimension. The maximum value of the fractal dimension was found to be 2.7872 assigned to sample SJ13 from the Upper Shajara Reservoir as verified in Table 1. Whereas the minimum value of the fractal dimension 2.4379 was reported from sample SJ3 from the Lower Shajara reservoir as displayed in Table1. The seismo magnetic field fractal dimension and capillary pressure fractal dimension were observed to increase with increasing permeability as proofed in Table1 owing to the possibility of having interconnected channels.

The Lower Shajara reservoir was denoted by six sandstone samples (Figure 1), four of which label as SJ1, SJ2, SJ3 and SJ4 were carefully chosen for capillary pressure measurement as established in Table1. Their positive slopes of the first procedure log of the seismo magnetic field (H) to maximum seismo magnetic field (Hmax) versus log wetting phase saturation (Sw) and negative slopes of the second procedure log capillary pressure (Pc) versus log wetting phase saturation (Sw) are explained in Figure 2, Figure 3, Figure 4, Figure 5 and Table 1. Their transverse relaxation time of nuclear magnetic resonance fractal dimension and capillary pressure fractal dimension values are revealed in Table 1. As we proceed from sample SJ2 to SJ3 a pronounced reduction in permeability due to compaction was described from 1955 md to 56 md which reflects decrease in seismo magnetic field fractal dimension from 2.7748 to 2.4379 as quantified in table 1. Again, an increase in grain size and permeability was proved from sample SJ4 whose seismo magnetic field fractal dimension and capillary pressure fractal dimension was found to be 2.6843 as pronounced in Table 1.

In contrast, the Middle Shajara reservoir which is separated from the Lower Shajara reservoir by an unconformity surface as shown in Figure 1. It was nominated by four samples (Figure 1), three of which named as SJ7, SJ8, and SJ9 as clarified in Table1 were chosen for capillary measurements as described in Table 1. Their positive slopes of the first procedure and negative slopes of the second procedure are shown in Figure 6, Figure 7 and Figure 8 and Table 1. Furthermore, their seismo magnetic field fractal dimensions and capillary pressure fractal dimensions show similarities as defined in Table 1.Their fractal dimensions are higher than those of samples SJ3 and SJ4 from the Lower Shajara Reservoir due to an increase in their permeability as explained in table 1.

On the other hand, the Upper Shajara reservoir was separated from the Middle Shajara reservoir by yellow green mudstone as shown in Figure 1. It is defined by three samples so called SJ11, SJ12, SJ13 as explained in Table 1. Their positive slopes of the first procedure and negative slopes of the second procedure are displayed in Figure 9, Figure 10 and Figure 11 and Table 1. Moreover, their t seismo magnetic field fractal dimension and capillary pressure fracal dimension are also higher than those of sample SJ3 and SJ4 from the Lower Shajara Reservoir due to an increase in their permeability as simplified in table 1.

Overall a plot of positive slope of the first procedure versus negative slope of the second procedure as described in Figure 12 reveals three permeable zones of varying Petrophysical properties. These reservoir zone were also confirmed by plotting seismo magnetic field fractal dimension versus capillary pressure fractal dimension as described in Figure 13. Such variation in fractal dimension can account for heterogeneity which is a key parameter in reservoir quality assessment.

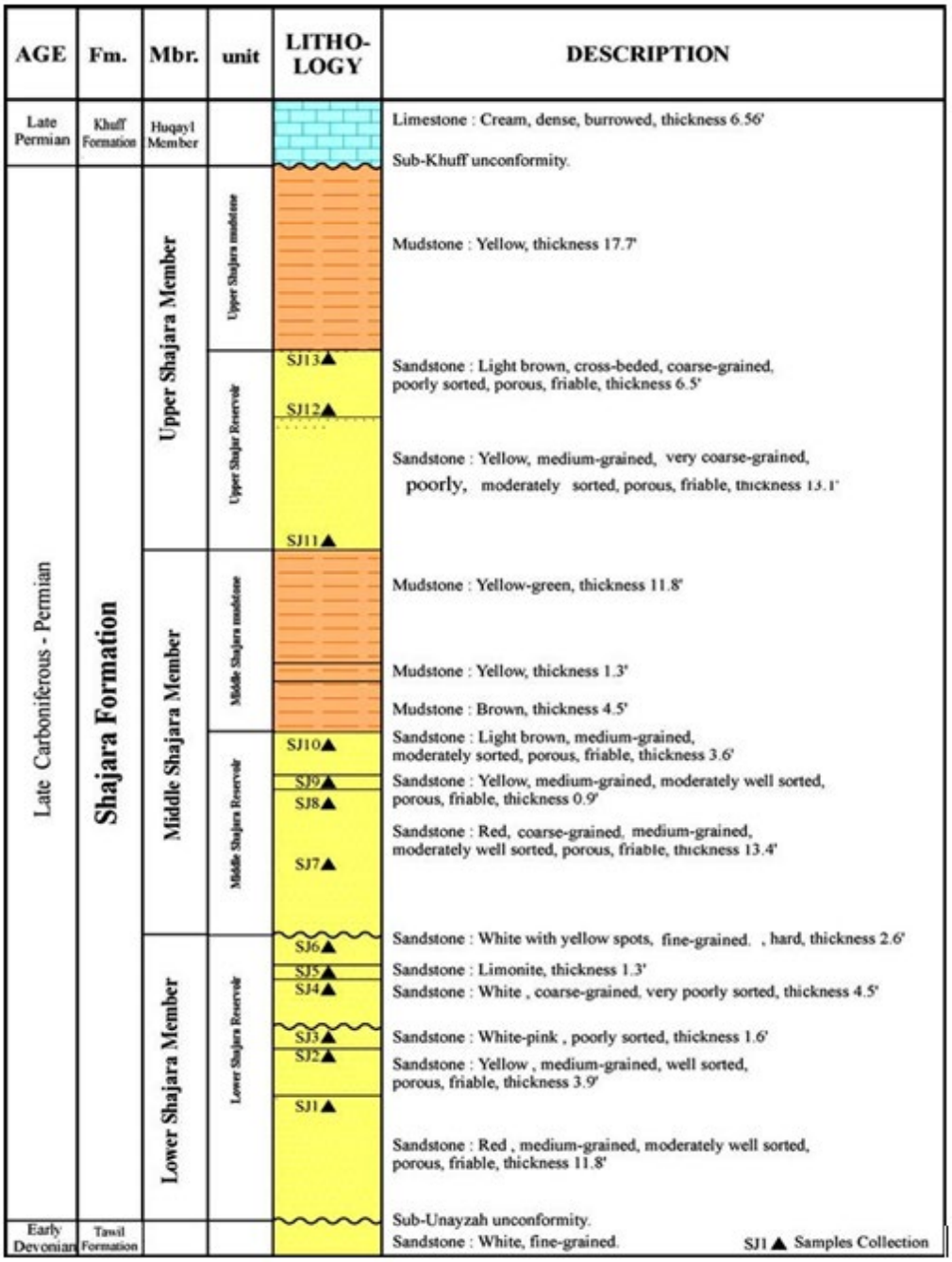

Figure 1: Surface type section of the Shajara Reservoirs of the Permo-Carboniferous Shajara Formation at latitude 26° 52' 17.4", longitude 43° 36' 18. ".

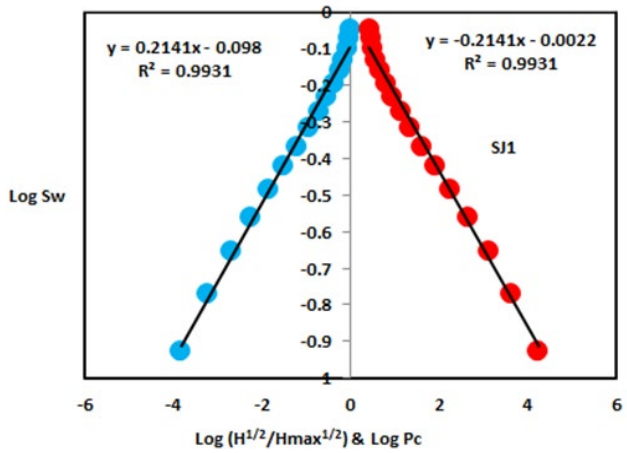

Figure 2: Log ($H^{1/2}/H^{1/2}max$) versus log Sw and log Pc versus log Sw of sample SJ1.

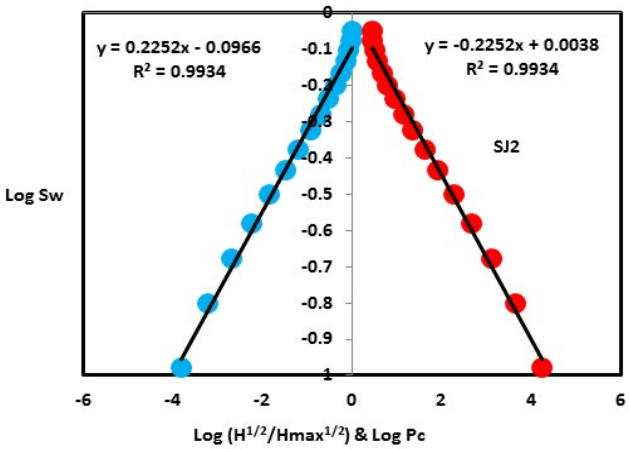

Figure 3: Log ($H^{1/2}/H^{1/2}max$) versus log Sw and log Pc versus log Sw of sample SJ2.

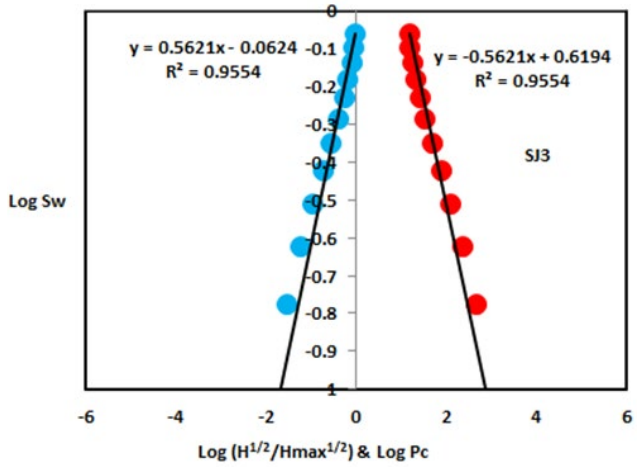

Figure 4: Log ($H^{1/2}/H^{1/2}max$) versus log Sw and log Pc versus log Sw of sample SJ3

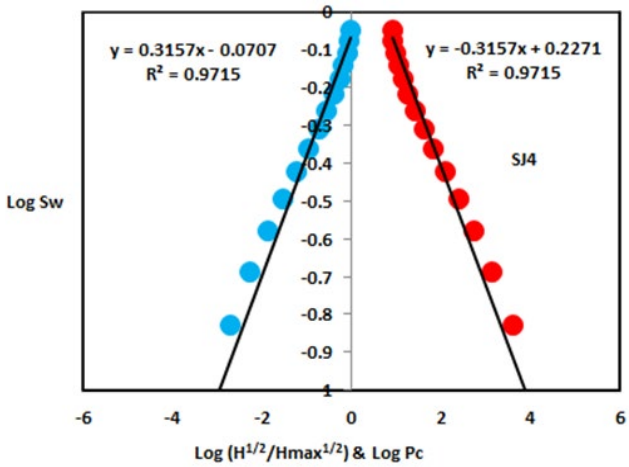

Figure 5: Log ($H^{1/2}/H^{1/2}max$) versus log Sw and log Pc versus log Sw of sample SJ4

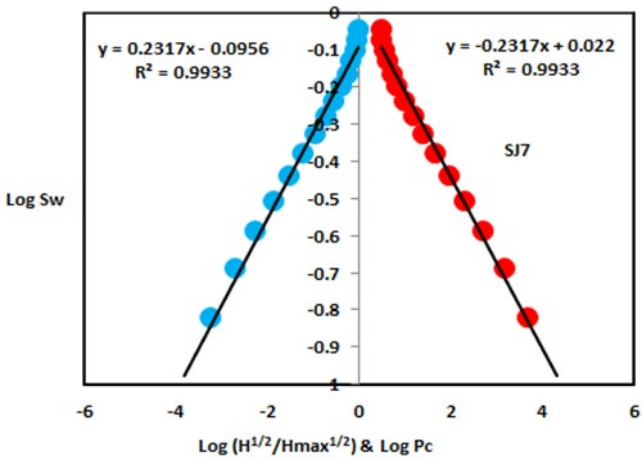

Figure 6: Log ($H^{1/2}/H^{1/2}max$) versus log Sw and log Pc versus log Sw of sample SJ7

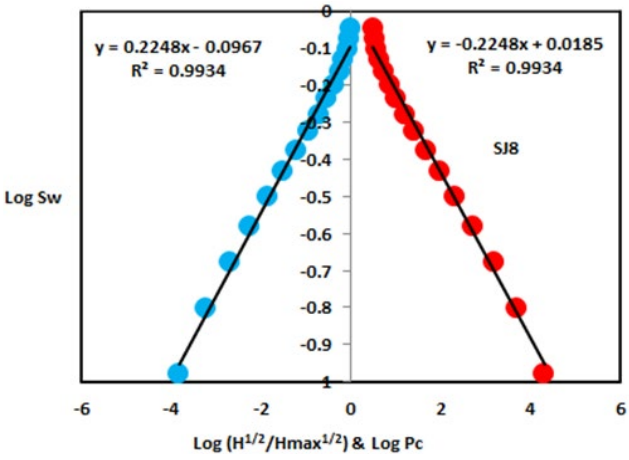

Figure 7: Log ($H^{1/2}/H^{1/2}max$) versus log Sw and log Pc versus log Sw of sample SJ8.

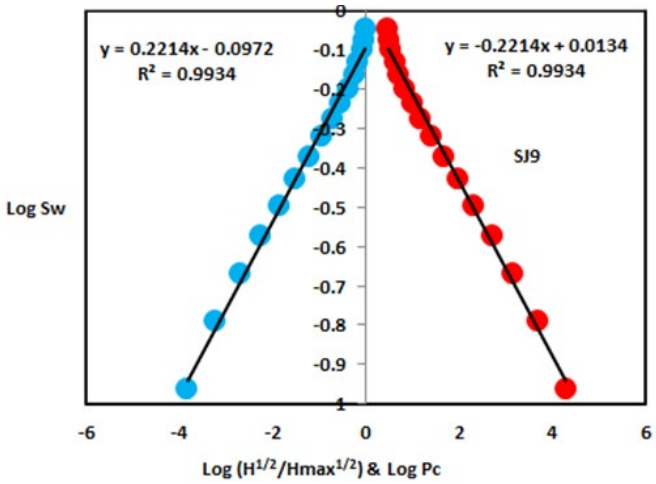

Figure 8: Log ($H^{1/2}/H^{1/2}max$) versus log Sw and log Pc versus log Sw of sample SJ9

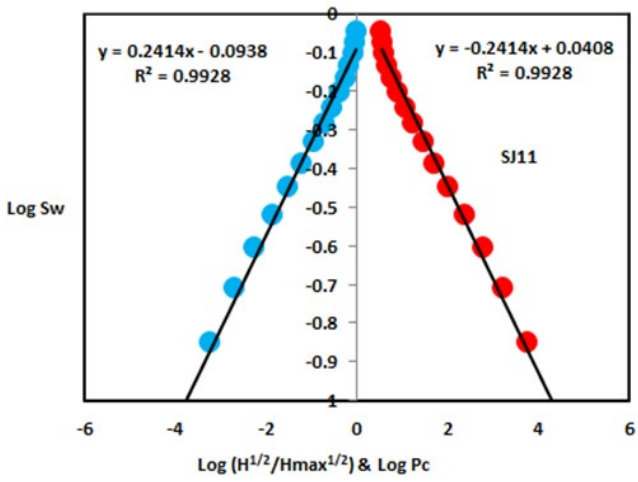

Figure 9: Log ($H^{1/2}/H^{1/2}max$) versus log Sw and log Pc versus log Sw of sample SJ11

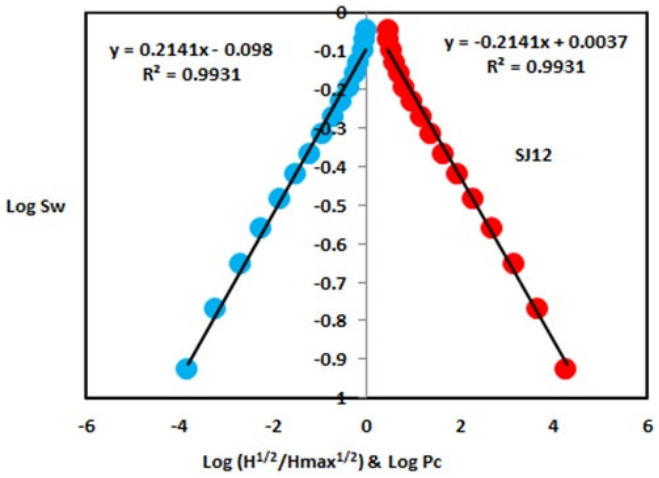

Figure 10: Log ($H^{1/2}/H^{1/2}max$) versus log Sw and log Pc versus log Sw of sample SJ12

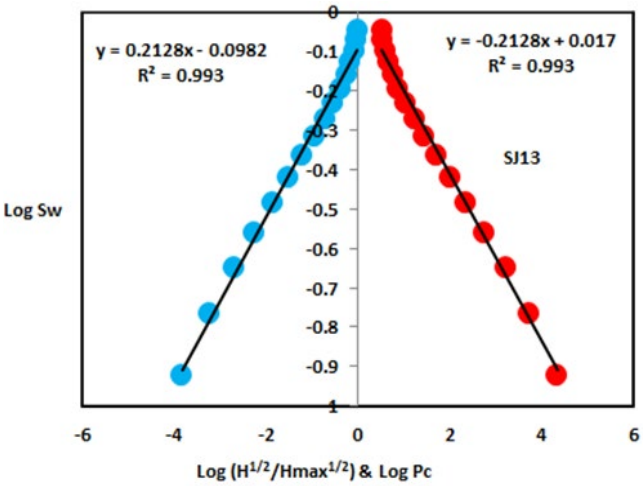

Figure 11: Log ($H^{1/2}/H^{1/2}max$) versus log Sw and log Pc versus log Sw of sample SJ13

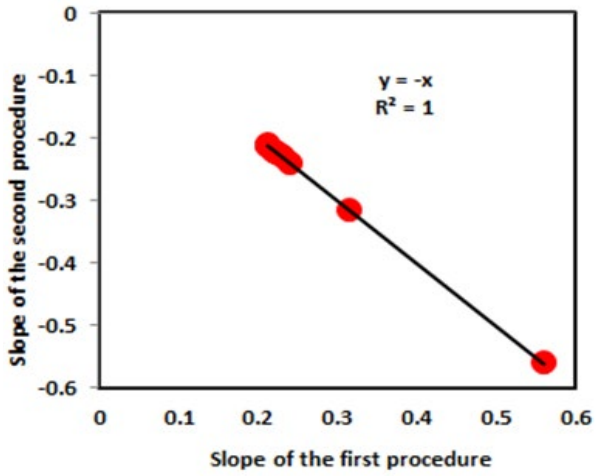

Figure 12: Slope of the first procedure versus slope of the second procedure

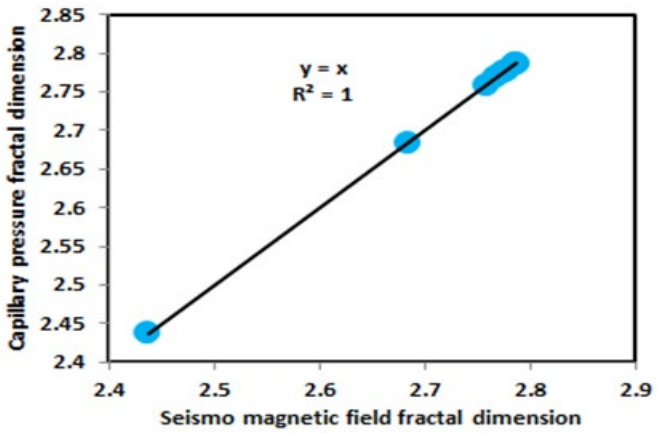

Figure 13: Seismo magnetic field fractal dimension versus capillary pressure fractal dimension

Formation	Reservoir	Sample	Porosity %	k (md)	Positive slope of the first procedure Slope=3-Df	Negative slope of the second procedure Slope=Df-3	Seismo magnetic field fractal dimension	Capillary pressure fractal dimension
Permo-Carboniferous Shajara Formation	Upper Shajara Reservoir	SJ13	25	973	0.2128	-0.2128	2.7872	2.7872
		SJ12	28	1440	0.2141	-0.2141	2.7859	2.7859
		SJ11	36	1197	0.2414	-0.2414	2.7586	2.7586
	Middle Shajara Reservoir	SJ9	31	1394	0.2214	-0.2214	2.7786	2.7786
		SJ8	32	1344	0.2248	-0.2248	2.7752	2.7752
		SJ7	35	1472	0.2317	-0.2317	2.7683	2.7683
	Lower Shajara Reservoir	SJ4	30	176	0.3157	-0.3157	2.6843	2.6843
		SJ3	34	56	0.5621	-0.5621	2.4379	2.4379
		SJ2	35	1955	0.2252	-0.2252	2.7748	2.7748
		SJ1	29	1680	0.2141	-0.2141	2.7859	2.7859

Table 1: Petrophysical model showing the three Shajara Reservoir Units with their corresponding values of seismo magnetic field fractal dimension and capillary pressure fractal dimension

Conclusion

The sandstones of the Shajara Reservoirs of the Shajara formation permo-Carboniferous were divided here into three units based on seismo magnetic field fractal dimension. The Units from base to top are: Lower Shajara seismo magnetic field Fractal dimension Unit, Middle Shajara Seismo Magnetic Field Fractal Dimension Unit, and Upper Shajara Seismo Magnetic Field Fractal Dimension Unit. These units were also proved by capillary pressure fractal dimension. The fractal dimension was found to increase with increasing grain size and permeability owing to possibility of having interconnected channels.

Acknowledgement

The author would to thank King Saud University, college of Engineering, Department of Petroleum and Natural Gas Engineering, Department of Chemical Engineering, Research Centre at College of Engineering, and King Abdullah Institute for research and Consulting Studies for their supports.

References

1. Frenkel, J. 1944. On the theory of seismic and seismoelectric phenomena in a moist soil. J physics 3(4): 230-241.

2. Li, K. and W. Williams, 2007. Determination of capillary pressure function from resistivity data. Transport in Porous Media 67(1): 1-15.

3. Revil A, Jardani A 2010 Seismoelectric response of heavy oil reservoirs: theory and numerical modelling. Geophysical J International 180(2): 781-797.

4. Dukhin, A., P. Goetz, M.Thommes, 2010. Seismoelectric effect: a non-isochoric streaming current. 1 experiment. J Colloid Interface Sci 345(2): 547-553.

5. Guan, W., H. Hu, Z .Wang, 2012. Permeability inversion from low-frequency seismoelectric logs in fluid- saturated porous formations. Geophysical Prospecting. 61(1): 120-133

6. Hu, H., W. Guan, W. Zhao, 2012. Theoretical studies of permeability inversion from seismoelectric logs. Geophysical Research Abstracts. 14: EGU2012-6725-1, 2012 EGU General Assembly 2012.

7. Borde C, S´en´echal P, Barri`ere J, Brito D, Normandin E, et al. 2015 Impact of water saturation on seismoelectric transfer functions: a laboratory study of co-seismic phenomenon. Geophysical J International 200(3): 1317-1335.

8. Jardani A, Revil A 2015 Seismoelectric couplings in a poroelastic material containing two immiscible fluid phases. Geophysical J International 202(2): 850-870.

9. Holzhauer, J., D . Brito, C. Bordes, Y.Brun, B. Guatarbes, 2016 Experimental quantification of the seismoelectric transfer function and its dependence on conductivity and saturation in loose sand. Geophys Prospect 65(4): 1097-1120.

10. Rong, P., W. Xing, D. Rang, D. Bo, L. Chun 2016. Experimental research on seismoelectric effects in sandstone. Applied Geophysics 13(3): 425-436.

11. Djuraev, U., S. Jufar, P. Vasant, 2017. Numerical Study of frequency-dependent seismoelectric coupling in partially-saturated porous media. MATEC Web of Conferences 87, 02001 (2017).

12. Alkhidir KEME 2017 Pressure head fractal dimension for characterizing Shajara Reservoirs of the Shajara Formation of the Permo-Carboniferous Unayzah Group, Saudi Arabia. Arch Pet Environ Biotech 2017 (2): 1-7.

13. Al-Khidir KE 2018 On Similarity of Pressure Head and Bubble Pressure Fractal Dimensions for Characterizing Permo-Carboniferous Shajara Formation, Saudi Arabia. J Indust Pollut Toxic. 1(1): 1-10.

14. Alkhidir KEME 2018 Geometric relaxation time of induced polarization fractal dimension for characterizing Shajara Reservoirs of the Shajara Formation of the Permo-Carboniferous Unayzah Group, Saudi Arabia. Scifed JPetroleum 2(1): 1-6.

15. Alkhidir KEME 2018. Geometric relaxation time of induced polarization fractal dimension for characterizing Shajara Reservoirs of the Shajara formation of the Permo-Carboniferous Unayzah Group-Permo. Int J Pet and Res. 2: 105-108.

16. Alkhidir KEME 2018. Arithmetic relaxation time of induced polarization fractal dimension for characterizing Shajara Reservoirs of the Shajara Formation. Nanosci and Nanotechnol. 1:1-8.

17. AlKhidir KEME 2018. Seismo Electric field fractal dimension for characterizing Shajara Reservoirs of the Permo-Carboniferous Shajara Formation, Saudi Arabia. Acad.j.Environ.Sci.6(5):113-120.

18. Alkhidir KEME 2018. Resistivity fractal dimension for characterizing Shajara reservoirs of the permo-carboniferous Shajara formation Saudi Arabia. Recent Adv Ptetrochem Sci.5(2):1-6.
19. Alkhidir KEME 2018. Electro Kinetic Fractal Dimension for Characterizing Shajara Reser¬voirs of the Shajara Formation. Arch Oil Gas Res.2018(1):1-7.
20. Alkhidir KEME 2018. Electric Potential Energy Fractal Dimension for Characterizing Permo-carboniferous Shajara Formation. Expert Opin Environ Biol. 7 (2): 1-5.
21. Alkhidir KEME 2018. Electric potential gradient Fractal Dimension for Characterizing Shajara Reservoirs of the Permo-Carboniferous Shajara Formation, Saudi Arabia. Arch Petro Chem Eng. 2018 (1): 1-6.
22. Alkhidir KEME 2018. On Similarity of Differential Capacity and Capillary Pressure Fractal Dimensions for Characterizing Shajara Reservoirs of the Permo-Carboniferous Shajara Formation, Saudi Arabia SF J Biofuel Bioenerg 1(2): 1-10.